Desalination and Water Treatment
www.deswater.com

doi:10.5004/dwt.2021.27215

225 (2021) 340–349
June

Effective removal of indigo-dyed batik by chemical activation and thermal treatment of banana peel waste coupled with magnetic magnetite particle

Duangdao Channei[a,b,*], Kantapat Chansaenpak[c], Panatda Jannoey[d], Hathaithip Sintuya[e], Wilawan Khanitchaidecha[f,b], Auppatham Nakaruk[g,b], Sukon Phanichphant[h]

[a]*Department of Chemistry, Faculty of Science, Naresuan University, Phitsanulok 65000, Thailand, email: duangdaoc@nu.ac.th*
[b]*Centre of Excellence for Innovation and Technology for Water Treatment, Naresuan University, Phitsanulok 65000, Thailand*
[c]*National Nanotechnology Center, National Science and Technology Development Agency, Thailand Science Park, Pathum Thani, Thailand 12120, email: kantapat.cha@nanotec.or.th*
[d]*Department of Biochemistry, Faculty of Medical Science, Naresuan University, Phitsanulok 65000, Thailand, email: panatdaj@nu.ac.th*
[e]*Asian Development College for Community Economy and Technology, Chiang Mai Rajabhat University, 50180, Thailand, email: hathaithip.nin@gmail.com*
[f]*Department of Civil Engineering, Faculty of Engineering, Naresuan University, Phitsanulok 65000, Thailand, email: wilawank@nu.ac.th*
[g]*Department of Industrial Engineering, Faculty of Engineering, Naresuan University, Phitsanulok 65000, Thailand, email: auppathamk@nu.ac.th*
[h]*Materials Science Research Center, Faculty of Science, Chiang Mai University, Chiang Mai 50200, Thailand, email: sphanichphant@gmail.com*

Received 22 September 2020; Accepted 7 March 2021

ABSTRACT

The magnetic adsorbent derived from banana peels (M-A-C-BP) with the high surface area was synthesized by thermal treatment and chemical activation. The M-A-C-BP composite contained crystalline magnetite (Fe_3O_4) which presented superparamagnetic properties. The presence of saturation magnetization in M-A-C-BP was similar to bare Fe_3O_4, indicating that Fe_3O_4 nanoparticles were successfully coated on the A-C-BP surface. The morphology obtained from the field-emission scanning electron microscope image revealed that the nanosized spherical Fe_3O_4 was uniformly dispersed on the A-C-BP surface, leading to a high Brunauer–Emmett–Teller specific surface area. The adsorption experiments were monitored via UV-spectrophotometric technique by varying the initial concentrations of indigo carmine (IC) from 10–100 ppm. The linear plot of the Langmuir isotherm equation indicated monolayer adsorption of M-A-C-BP toward IC molecules with the maximum monolayer capacity (Q_m) value of 8.72 mg/g. The chemisorbed IC on M-A-C-BP could be described by the pseudo-second-order kinetic model. The easy recovery of magnetic adsorbent M-A-C-BP represented its practical application in IC removal from aqueous solution by an external magnetic field, which was investigated over five consecutive adsorption cycles.

Keywords: Banana peel; Adsorption; Magnetic adsorbent; Indigo carmine; Fe_3O_4

* Corresponding author.

1. Introduction

In the southern region of Thailand, domestic textiles are very popular. They are usually passed from generation to generation and known locally as batik industries. Because of high domestic as well as international demand, the batik industry has a significant influence on economic development in the local area. As a lot of chemicals are used in the production processes, the batik industry ends up releasing industrial wastewater into the environment. In addition to dyes, batik wastewater also contains artificial ingredients, including, grease, wax, heavy metal, and surfactant, which are difficult to decompose.

Typically, remazol black, indigo, red and golden yellow are general dyes used in the textile industries [1]. Their existence in nature can cause environmental problems, as they are hard to degrade and can cause an increase in chemical oxygen demand (COD), biochemical oxygen demand, and total suspended solids levels in natural water. Technically, only about 5% of these compounds are used in the coloring process, so that the remaining 95% of dyes are discarded as liquid waste [2]. Without appropriate treatment, dye-containing batik wastewater discharged into the waste stream could cause a significant effect on the environment. Due to the fact that the colors in industries are non-biodegradable wastes, many researchers are interested in finding the appropriate methods to treat the color-containing wastewater.

Recently, several technologies have been invented for the treatment of organic contaminants such as sedimentation, membrane filtration, electrochemical oxidation, coagulation, biological process, and adsorption. These methods have attracted much attention in recent years due to their simplicity of design and easy operation [3–5]. For example, Lin and Liu [6] reported the combination of ozonation and coagulation methods for the treatment of material wastewater. The results demonstrated that ozonation could effectively remove the textile wastewater within 10 min in the batch experiment. Likewise, coagulation removed dissolved and suspended solids with a COD removal efficiency of up to 66%.

Additionally, Reynolds et al. [7] examined different sorts of color wastewater using biological processes. They found that the COD value, as well as the color contaminants, could not be effectively degraded by this method. Next, Bell et al. [8] decolorized color wastewater utilizing an anaerobic baffled reactor. It decreased in COD of 50%–60% with decolorization efficiency of around 95%. Also, Viraragahan and Ramakrishna [9] reported the effect of different four concentrations of synthetic dyes on the adsorption capacity of the different particles sizes of fly ash. However, the mentioned procedures used the adsorbents that could not be recovered and reused. To address this issue, the decolorization and mineralization of batik wastewater with low-cost adsorbents coupled with magnetic magnetite particles for the sake of recovery are the primary aim of this research.

Gupta et al. [10] reported a comprehensive review on the variety of possible low-cost adsorbents, including, clay materials, bentonite, kaolinite, silica, zeolites, alunite, perlite, waste carbon slurries, and metal hydroxide sludge. The prepared adsorbents were mainly used without chemical/physical activations, but in some cases, the treatment with hydrolyzing chemicals could yield the adsorbents with high surface area, high porosity and specific chemical properties. The investigations on the adsorption properties of the alternative low-cost adsorbents were widely applied for the removal of risky contaminations from industrial wastewaters, such as, heavy metals from electroplating wastewaters and dyes/colors from textile wastewater.

Lately, specific focus has been given to the use of available-in-nature, abundant, and eco-friendly adsorbents to replace traditional and costly adsorbents. In Thailand, a large portion of waste, especially fruit or food wastes, has been widely found all over the country. Therefore, the recycling of such wastes to produce activated carbon/charcoal for the adsorbent applications could be an eco-friendly method the reduce those waste in the areas. In addition, the adsorbents synthesized from agricultural wastes takes advantage not only in term of cost-effectiveness due to inexpensive and readily available precursors but also in term of agricultural waste management [11–15].

As presented in Table 1, various types of agricultural wastes including coconut shells, wheat straw, rice husk, bamboo chips, pokeweed plants, sugarcane bagasse, and other types of biomass have been used to produce activated carbon adsorbents which are then applied to wastewater treatment. Those activated carbons can effectively adsorb organic molecules, such as methylene blue, phenol, 2,4,6-trichlorophenols, fluoride, hexavalent chromium, and lead ion.

There are two methods to synthesize activated carbons, defined as physical and chemical activations. In the physical activation, raw material is converted to a char by carbonization in an inert atmosphere at temperatures less than 700°C. After that, steam or carbon dioxide is introduced at temperatures of 800°C–900°C steam to develop an internal porous structure in the char. On the other hand, in the chemical activation, the carbonization stage and the activation stage are combined, in which chemicals such as acids (HNO_3, HCl, H_2SO_4, H_3PO_4, etc), base (NaOH, KOH, etc), and salts ($NaNO_3$, KNO_3, etc) are mixed with the raw material, prior to heating at high temperature in the absence of oxygen. The chemical activation method provides several advantages, such as lower operating temperature and ease of surface modifications with specific functional groups to increase the adsorption efficiency of specific pollutants [10,23–25]. With the goal to enhance separation performance, the prepared adsorbents can be modified with iron oxide in the magnetite phase (Fe_3O_4) to add the magnetic property to the materials and make them more recyclable and maintainable. This progressing improvement is driven by the fast-industrial growth in various regions of the world accompanied by expanding environmental pollution and examining for low-cost resolutions for these issues.

In this study, the activated charcoal (A-C-BP) was prepared from the carbonized banana peel waste biomass by acid activation followed by magnetization with Fe_3O_4 nanoparticles. This synthesized magnetic banana peel-activated carbon composite (M-A-C-BP) was then used for the adsorption of indigo carmine (IC).

Table 1
Applications of adsorbents from biomass in wastewater treatment

Pollutants	Type of adsorbents	Precursors	Synthesis method	Adsorption capacity	References
Methylene blue	Activated carbons	Bamboo chips	Steam activation	250 mg/g	[16]
Methylene blue	Activated carbons	Coconut shell	–	80% of Methylene blue removal, 120 min	[17]
Fluoride	Sawdust	Sawdust	Formaldehyde treatment	50% of fluoride removal, 60 min	[18]
Phenol	Activated carbons	Pokeweed plants	Chemical activation	172 mg/g	[19]
Hexavalent chromium	Carbonaceous adsorbents	Sunflower heads	Sulfuric acid treatment and carbonization at 150°C	75.7% of Cr^{6+} removal, 2 h (heads)	[20]
		Sunflower stems		85.4% of Cr^{6+} removal, 2 h (stems)	
2,4,6-trichlorophenols	Activated carbons	Coconut husk	KOH activation	716 mg/g	[21]
Lead ion (Pb^{2+})	Zeolite	Rice husk ash	–	85% of Pb^{2+} removal, 24 h	[22]

2. Materials and methods

2.1. Activated charcoal as an adsorbent

The adsorbent was prepared from the banana peel (BP), collected from local agricultural fields around Sukhothai Province, Thailand, and was cut into small pieces, washed, and dried in a hot air oven for 24 h at 120°C to remove moisture (dried BP, D-BP), followed by impregnation in 6 M H_2SO_4 for 24 h (ratio: 25 g/200 mL), labeled as A-BP. The impregnated A-BP was heated in a muffle furnace at 500°C and maintained at this temperature for 1 h (A-C-BP). For comparison, the dried BP was transferred to a muffle furnace without acid activation (C-BP). All samples were further analyzed by N_2 adsorption/desorption based on Brunauer–Emmett–Teller (BET) theory to compare the capacity of adsorption in terms of specific surface area. The selected sample with the highest specific surface area was further combined with magnetic Fe_3O_4 nanoparticles.

2.2. Magnetization of the prepared activated carbon (M-A-C-BP)

0.01 mmol (2.7800 g) of $FeSO_4$ and 0.02 mol (5.4060 g) of $FeCl_3$ were dissolved in 80 mL of distilled water, and then 0.25 g of the selected A-C-BP powder was added. After that 20 mL of 0.08 mol, NaOH solution was added dropwise to precipitate the hydrated iron oxides, as the chemical reaction shown in Eq. (1):

$$FeSO_4 + 2FeCl_3 + 8NaOH \rightarrow Fe_3O_4 + Na_2SO_4 + 6NaCl + 4H_2O \quad (1)$$

The suspension was mixed under a magnetic stirrer for 1 h at 100°C. After cooling, the mixture was washed repeatedly with DI water until the pH became neutral. The magnetized activated carbon derived from the banana peel (M-A-C-BP) was separated by centrifugation, dried at 120°C for 24 h and stored in an airtight container.

2.3. Characterizations of M-A-C-BP

The prepared M-A-C-BP was characterized for its surface morphology by field-emission scanning electron microscope linked with energy-dispersive X-ray spectroscopy (FE-SEM/EDS: JSM-6335). The crystal structure and phase composition of Fe_3O_4 before and after combined with A-C-BP were recorded by X-ray diffraction (XRD, Philips X'Pert MPD Licensed by Philips/PANalytical Company, Netherlands) using Cu K-alpha radiation. Specific surface area, pore volume and pore diameter were analyzed by N_2 adsorption/desorption isotherm based on the theory of BET (Micromeritics TriStar II 3020, Micromeritics Company, USA). The magnetic property was characterized by a vibrating sample magnetometer (VSM, Lake Shore Model 7404) at room temperature. Also, the points of zero charge/zeta potential of the prepared adsorbent were determined by the zeta potential analyzer (Malvern Zetasizer Licensed by Malvern Company, United Kingdom).

2.4. Batch adsorption experiments

2.4.1. Equilibrium experiments

For batch adsorption experiments, adsorption equilibrium experiments were carried out by varying the indigo-dyed batik (indigo carmine, IC) concentrations of 10, 20, 60, and 100 ppm (mg/L). The adsorbent dosage was fixed as 0.1 g suspended in 50 mL of dye aqueous solution. The decrease of dye concentration as well as the decrease in absorbance intensity with the different adsorption times (0, 30, 60, 90, and 120 min) was monitored using double beam UV/Vis (Shanghai Mapada Instruments Co., Ltd., China) at the absorbance of IC around 615 nm. The M-A-C-BP particles were magnetically separated from the suspension using an external magnetic field. The amount of adsorption of IC at various contacting time (t) intervals were calculated by Eq. (2):

$$Q_t = \frac{(C_i - C_t)V}{W} \quad (2)$$

where Q_t (mg/g) is the adsorption capacity at time t. C_i and C_t (ppm) are the initial concentration and the remaining concentration of IC at a different time intervals, which are obtained from a linear calibration curve. V is the volume of IC solution (L), and W is the mass of M-A-C-BP used (g).

The amount of IC adsorbed at equilibrium, Q_e (mg/g) was generally calculated by the equilibrium concentrations of IC (C_e, ppm), as shown in Eq. (3) [26]:

$$Q_e = \frac{(C_i - C_e)V}{W} \quad (3)$$

where C_e and Q_e were modeled with Langmuir and Freundlich isotherms with the linear form of these two isotherms are shown in Eqs. (4) and (5), respectively [27]:

$$\frac{C_e}{Q_e} = \frac{1}{K_L Q_m} + \frac{C_e}{Q_m} \quad (4)$$

$$\log Q_e = \log K_F + \frac{1}{n}\log C_e \quad (5)$$

2.4.2. Kinetic experiments

The kinetic data were modeled with pseudo-first-order equation and pseudo-second-order equation. The proposed method for analyzing the kinetics of the adsorption process namely pseudo-first-order equation can be expressed in its linear form as Eq. (6) [28]:

$$\log(Q_e - Q_t) = \log Q_e - \frac{k_1}{2.303}t \quad (6)$$

For the pseudo-second-order rate, the linear equation can be expressed as Eq. (7):

$$\frac{t}{Q_t} = \frac{1}{k_2 Q_e^2} + \frac{1}{Q_e}t \quad (7)$$

where k_1 (min^{-1}) and k_2 (g/mg min) are the rate constant of pseudo-first-order adsorption and pseudo-second-order adsorption, respectively.

3. Results and discussion

3.1. Characterizations of adsorbents

Surface properties obtained from the N_2 adsorption/desorption isotherms, pore-volume, and the pore size distributions for the four kinds of adsorbents are summarized in Table 2. The specific surface area (SSA) of dried BP (D-BP) without chemical activation was obtained at 0.75 m^2/g. However, a slight increase of SSA of 0.79 and 3.197 m^2/g was obtained in A-BP and C-BP samples, respectively. The sample prepared with both chemical activation and carbonization processes (A-C-BP) exhibited the highest SSA (215.05 m^2/g) and the largest pore volume (0.0497 cm^3/g) in the series, which was beneficial for the adsorption process. The pore size distributions of all adsorbents mainly fell into the range of mesopores (1–50 nm). After H_2SO_4 treatment, a great amount of collapsed structures of fiber and cellulose contents on the D-BP surface changed to a carbon-rich structure with the higher surface area which is favorable for adsorption [29]. Heat treatment at 500°C transferred more volatile and ash contents into the mixture of carbon and the remaining H_2SO_4 solution was released into the air which creates a pore network. The extremely high SSA can be achieved by the combined methods between the chemical activation and the carbonization as seen in the A-C-BP sample. Therefore, the A-C-BP was selected to be further prepared as a magnetic adsorbent (M-A-C-BP) through the simple redox reaction between $FeSO_4$ and $FeCl_3$.

Table 2
Surface properties

Sample	SSA area (m^2/g)	Pore volume (cm^3/g)	Pore size (nm)
D-BP	0.75	0.0004	8.49
A-BP	0.79	0.0009	5.05
C-BP	3.97	0.0111	16.19
A-C-BP	215.05	0.0497	5.78

X-ray diffraction technique and magnetic property measurement were then used to confirm the existence of Fe_3O_4 in M-C-A-BP composite. The XRD patterns of Fe_3O_4 and M-C-A-BP are presented in Fig. 1. The Fe_3O_4 reflections of [111], [220], [311], [400], [422], [511], [440], [620], and [533] are figured out at 2θ = 18.4°, 30.2°, 35.6°, 43.2°, 53.6°, 57.3°, 62.5°, 70.9°, and 73.8°, respectively, which match well with the database of magnetite in the JCPDS card number 190629 [30]. No other peaks due to maghemite (Fe_2O_3) was detected in this pattern. For the magnetic adsorbent sample (M-C-A-BP), the XRD pattern of Fe_3O_4 was still found as the major phase which is not seen in the A-C-BP sample confirming the presence of magnetite structure in M-C-A-BP.

Afterwards, magnetic properties of the prepared Fe_3O_4 and M-A-C-BP were measured at room temperature, as shown in Fig. 2. The observed hysteresis loops were not detected in the curves suggesting the superparamagnetism behavior of the prepared Fe_3O_4 with 70.29 emu/g saturation magnetization intensity [31]. For the M-A-C-BP sample, the magnetization value was obtained as 40.72 emu/g proving the complete combination of the composite between Fe_3O_4 and A-C-BP. The magnetism of M-A-C-BP was also confirmed by applying the external magnetic bar. This magnetic adsorbent can be effectively separated from the suspension yielding a clear solution within 20 s. Without Fe_3O_4, the A-C-BP adsorbent did not present magnetism when subjected to external magnetic fields. These results can further confirm the presence of Fe_3O_4 in the M-A-C-BP composites. Therefore, the M-A-C-BP composites offer a convenient way to recycle the magnetic adsorbent after the adsorption experiment by applying an external magnetic field.

Next, the scanning electron microscope and energy-dispersive X-ray spectroscopy (EDS) was used to reveal the

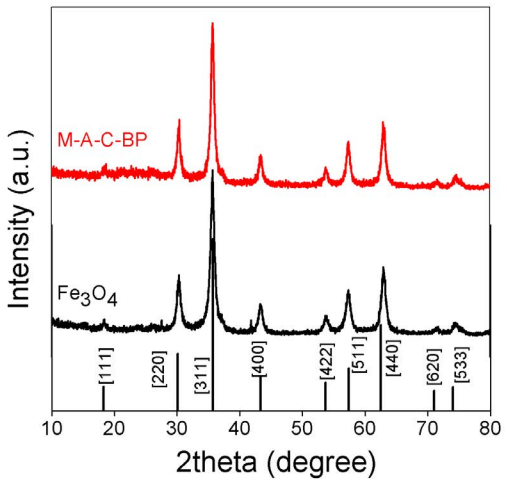

Fig. 1. Comparison of XRD patterns for Fe_3O_4 and M-C-A-BP samples.

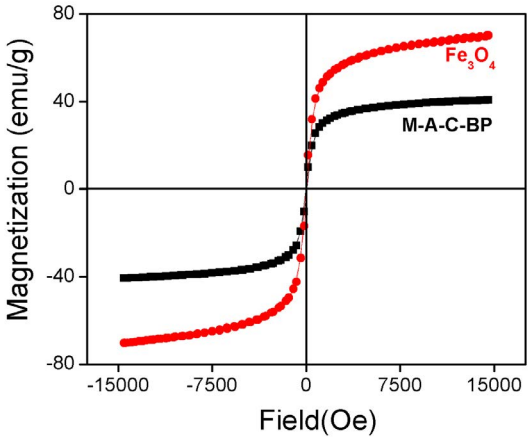

Fig. 2. Room-temperature magnetization curve of Fe_3O_4 and M-A-C-BP.

morphology and the elemental analysis of the magnetic adsorbent compared with Fe_3O_4 nanoparticles, respectively. As demonstrated in Fig. 3a, Fe_3O_4 nanoparticles exhibited aggregated spherical shapes with particle size smaller than 100 nm. In addition, Fig. 3b shows the porous form in the A-C-BP sample, which is essential in the production of adsorbent. Figs. 3c and d reveal the uniform mixture of Fe_3O_4 nanoparticles on the A-C-BP surface under different magnifications. The EDS spectrum demonstrated in Fig. 3e disclosed the presence of Fe and O which agreed well with the characteristic of Fe_3O_4. As shown in Fig. 3f, the major elements found in Fe_3O_4/A-C-BP composite are carbon, iron, and oxygen confirming the presence of Fe_3O_4 in the M-A-C-BP sample. At energies below ~2.5 keV, the strong peaks of Au were detected as the sample was coated with a layer of gold for this analysis.

Then, the zeta potentials at a pH range of 2–12 were used to study the effect of surface charge on adsorption of negatively charged IC on A-C-BP and M-A-C-BP. Based on the zeta potential graph in Fig. 4a, the points of zero charge (pzc) of A-C-BP and M-A-C-BP were discovered at pH 4.1 and 5.0, respectively. Since the natural pH of indigo carmine solution is 9, the zeta potentials of the prepared materials were focused on this pH. As seen in Fig. 4a, the positively charged surface was found in M-A-C-BP while the negatively charged surface was observed in A-C-BP at pH 9. This result suggested the strong electrostatic interaction between the positively charged surface of M-A-C-BP and the negative charge of anionic IC.

To clarify this issue, the adsorption capacity (Q_e, mg/g) with increasing NaCl concentrations or ionic strength (I) was investigated at the equilibrium time of 60 min. In this experiment, the prepared adsorbents were subjected to adsorb with IC in the mixed solutions with different ionic strengths (NaCl concentration range between 0.1 to 1.0 M). This adsorption behavior at different ionic strengths (I) can confirm the electrostatic interactions between the surface of absorbents and the negative charge of IC dye at the natural pH of IC dye (pH 9).

The adsorptions of IC dye on A-C-BP with the function of the ionic strengths are depicted in Fig. 4b. The adsorption capacity of A-C-BP was increased with the increase of ionic strength. This result indicated that the electrostatic interaction between the A-C-BP surface and the IC is repulsive, which corresponded to zeta potential analysis. In the case of M-A-C-BP, the adsorption capacity of negatively charged IC molecules on positively charged surface of M-A-C-BP with the function of ionic strength at pH 9 get decreased suggesting attractive electrostatic interactions. These results are consistent with the research of López-Ramón et al. [32] in which they studied the effect of ionic strength toward adsorption between the carbon surface and the metal ions. In addition, an increase in the ionic strength of the solution could reduce intermolecular electrostatic interactions, either repulsive or attractive, due to a screening effect of the electrolyte as seen in the literature [33,34].

3.2. Adsorption results

All the adsorption experiments in this study were carried out using M-A-C-BP at room temperature (300.15 K). The influence of initial IC concentrations was studied by varying concentrations from 10 to 100 ppm to determine the capacity of the prepared M-A-C-BP. Fig. 5a presents the remaining concentration of IC (C_t, ppm) plotted with various contact time intervals. All adsorption rates were fast during the first 30 min, and the adsorption approached equilibrium within 60 min in all the cases. The equilibrium concentrations (C_e) ranged from 3.90, 7.61, 31.00, and 78.15 ppm for initial IC concentration of 10, 20, 60, and 100 ppm, respectively. Generally, the adsorption capacity of the amount of adsorbate adsorbed at equilibrium reported in term of Q_e (mg/g), which can be calculated from C_i and C_e, as shown in Eq. (3) in materials and methods section. The Q_e values were calculated as 4.55, 8.37, 14.32, and 8.46 mg/g for 10, 20, 60, and 100 ppm, respectively. The corresponding values of Q_e was also determined by a plot of Q_t vs. time, as shown in Fig. 5b.

It was found that the adsorption capacity of the adsorbent increased with the increasing amount of initial IC

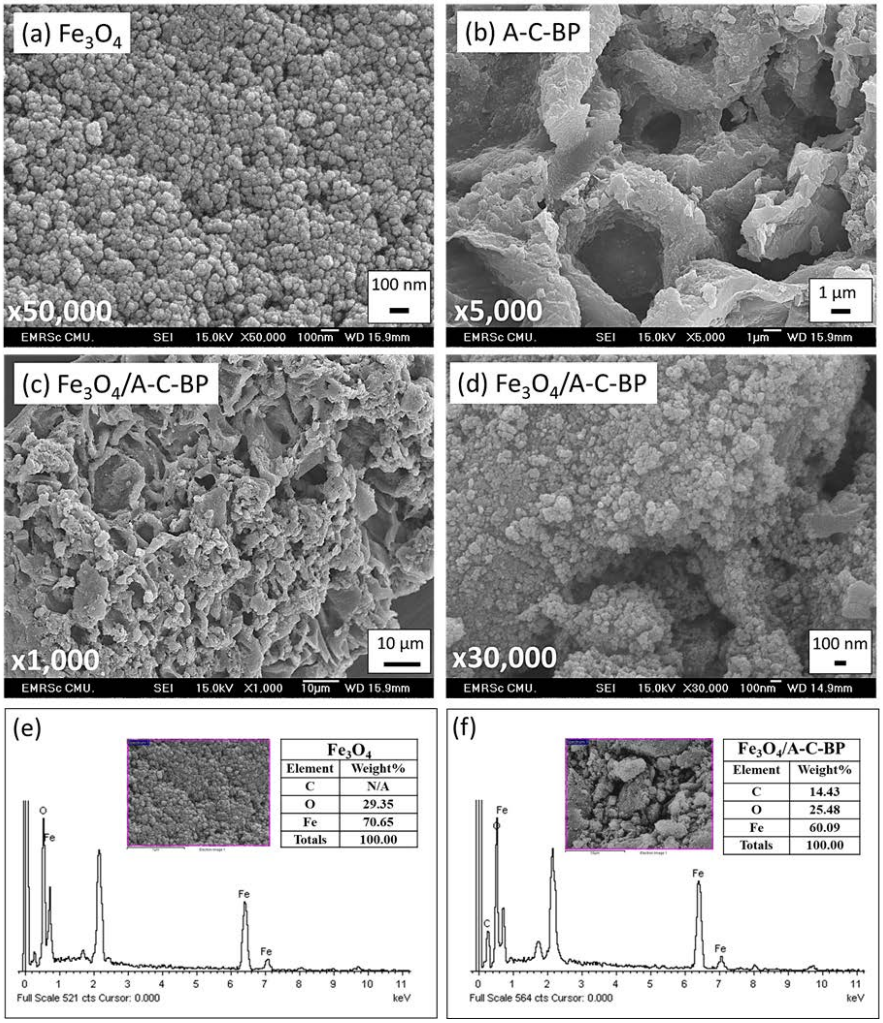

Fig. 3. Field-emission scanning electron microscope image of (a) Fe_3O_4, (b) A-C-BP, (c and d) Fe_3O_4/A-C-BP and EDS spectrum of (e) Fe_3O_4 and (f) Fe_3O_4/A-C-BP.

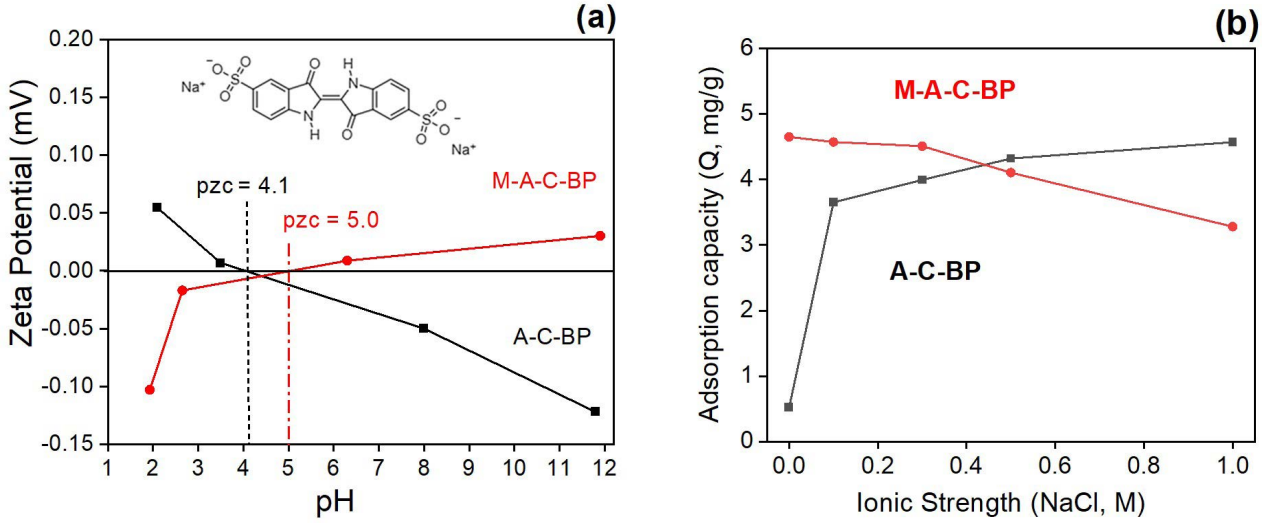

Fig. 4. (a) Zeta potential of A-C-BP, M-A-C-BP and chemical structure of IC and (b) effect of ionic strength on the adsorption capacity at pH 9 (ads. dosage = 0.1 g/50 mL of 10 ppm IC; adsorption time = 60 min; T = 300.15 K).

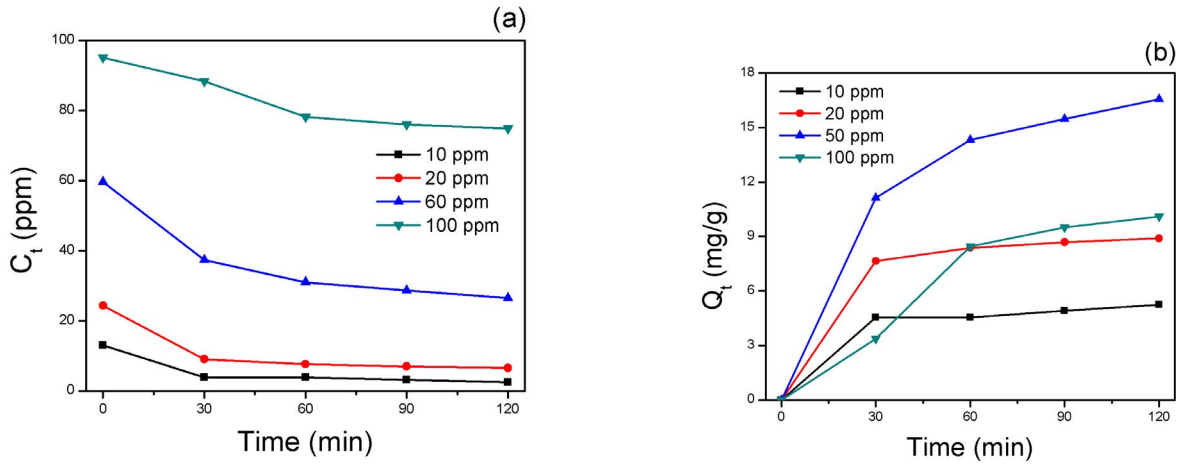

Fig. 5. (a) The remaining concentration on the time (C_t) and (b) adsorption capacity (Q_t) (ads. dosage = 0.1 g/50 mL; T = 300.15 K).

concentrations at concentrations up to 50 ppm suggesting that the adsorbate concentration is directly proportional to the adsorption capacity of the adsorbent. However, the adsorption capacity at the initial IC concentration of 100 ppm is lower than that of 50 ppm. This is because, at low initial concentrations (10–50 ppm), the active sites of adsorbent are not saturated with the IC molecules, yet. Therefore, the adsorbent can effectively absorb IC at these concentrations. On the other hand, at a high initial concentration such as 100 ppm, the available active sites of adsorbent are saturated with the IC molecules leading to lower adsorption capacity.

This may be explained by the mechanism of adsorption through three steps: (i) transport of IC molecules from solution to the surface of the adsorbent, (ii) the intraparticle diffusion of IC molecules into the certain pores of the adsorbent, and (iii) the adsorption in the pore interior with the slow adsorption rate due to less IC concentration in the solution and/or the unavailability of active sites of adsorbent [35,36].

Typically, the recycling of the magnetic adsorbent (M-A-C-BP) is an economic necessity. 10 ppm of IC solution with 120 min adsorption time were used for the regeneration of M-A-C-BP for all recyclable times. The highest desorption efficiency was found to be 86.86% at the first cycle (Fig. 6). The adsorption cycles were repeated 5 times using the same batch of M-A-C-BP separated by applying an external magnetic field.

M-A-C-BP exhibited good stability and reusability over 5 consecutive adsorption cycles with only 18% decrease in adsorption efficiency compared with the first run. The recycle test was analyzed up to only 5 cycles because the M-A-C-BP the magnetic adsorbent could not be easily separated by an external magnetic field after the fifth cycle and some A-C-BP particles were lost during the magnetic separation.

The equilibrium data were compared with the plots of Langmuir and Freundlich isotherms, as given in Figs. 7a and b respectively. The obtained isotherm parameters from these two isotherms are listed in Table 3. The correlation coefficient of the linear Langmuir adsorption isotherm (R^2 = 0.9353) showed a better fit with the IC adsorption data than that of linear Freundlich expression (R^2 = 0.1407). Therefore, it could be inferred that the adsorption behavior of IC on the heterogeneous surface of M-A-C-BP is associated with monolayer adsorption. In addition, since the values of $1/n$ in the Freundlich parameter was less than 0.5, it could be implied that the Langmuir model is more favorable [37]. The maximum monolayer capacity (Q_m) calculated from the slope of the Langmuir equation was about 8.72 mg/g.

The kinetic data for all the four initial IC concentrations were plotted for pseudo-first-order and pseudo-second-order equations, as given in Fig. 8, and the parameters obtained from these linear equations are presented in Table 4. Compared among the R^2 values for linear regression, it was found that the R^2 values of pseudo-second-order equation were higher than those of pseudo-first-order for all concentrations of the adsorbate except for the concentration at 100 ppm. In addition, the Q_e (calculated) obtained from the kinetic linear plots were comparable with the Q_e (experimental) values from the batch adsorption experiments. This implied that the adsorption of IC onto M-A-C-BP was chemisorption through a chemical bond between the functional groups in M-A-C-BP and IC molecules [38].

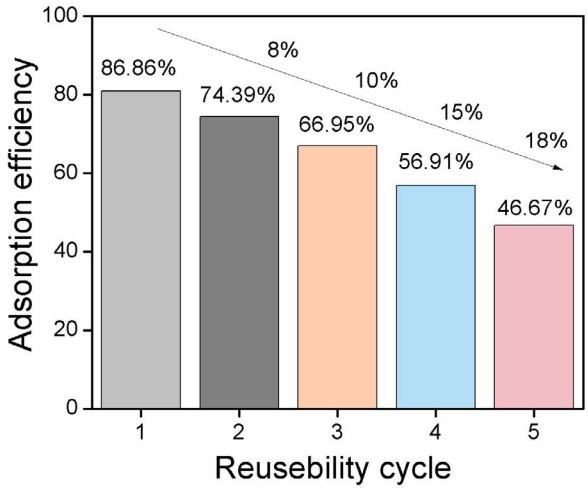

Fig. 6. Reusability for dye adsorption onto M-A-C-BP (ads. dosage = 0.1 g/50 mL; T = 300.15 K).

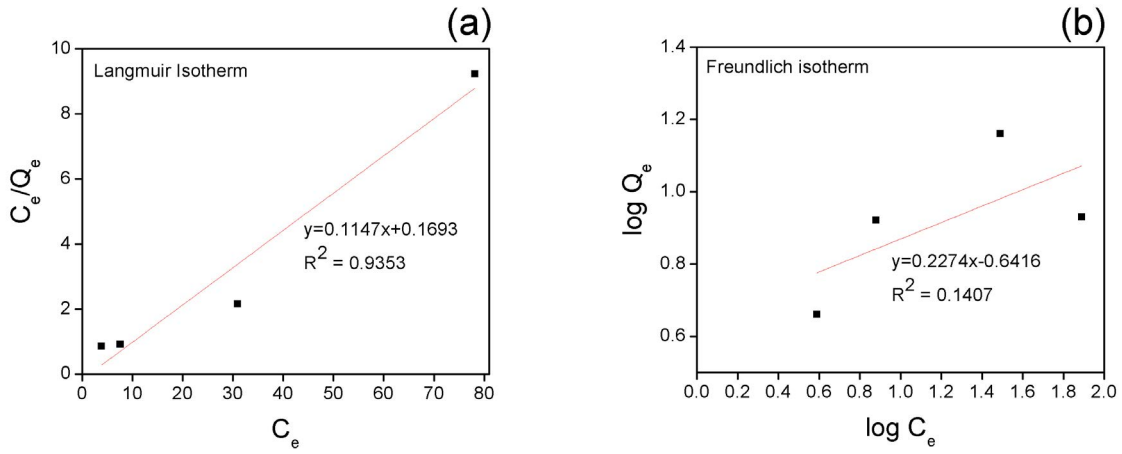

Fig. 7. Comparative of linearized isotherm models (a) Langmuir and (b) Freundlich isotherms.

Table 3
Langmuir and Freundlich adsorption parameters

Langmuir			Freundlich		
Q_m (mg/g)	K_L (L/mg)	R^2	K_F (L/mg)	$1/n$	R^2
8.72	0.68	0.9353	0.23	0.2274 × ($1/n$ < 0.5)	0.1407

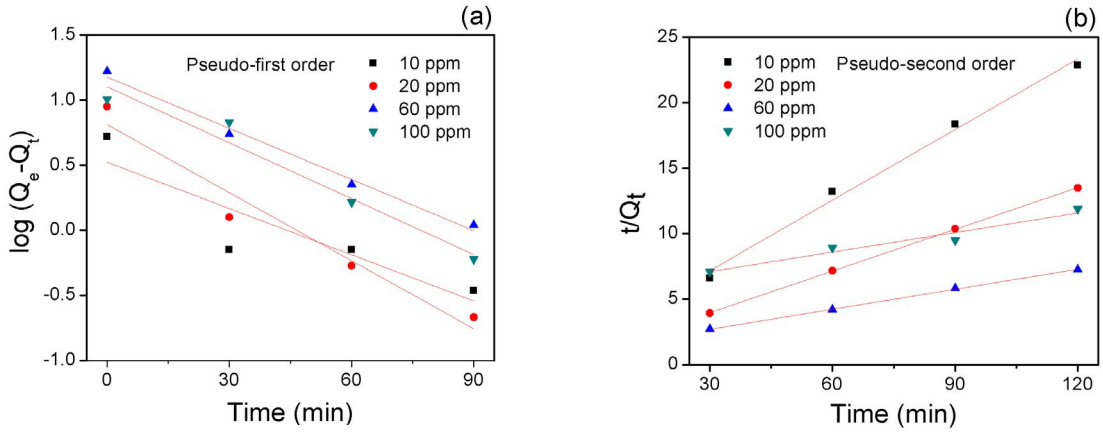

Fig. 8. Linear (a) pseudo-first-order and (b) pseudo-second-order plot for adsorption.

Table 4
Kinetic model parameters

Parameters	Initial indigo carmine concentration			
	10 ppm	20 ppm	60 ppm	100 ppm
Pseudo-first-order model				
k_1 (min^{-1})	0.0272	0.0401	0.0302	0.0329
Q_e, calculated (mg/g)	3.32	6.46	14.96	12.60
Q_e, experimental (mg/g) at 60 min	4.55	8.37	14.32	8.46
R^2	0.7149	0.9322	0.9857	0.9439
Pseudo-second-order model				
k_2 (g/mg min)	0.0181	0.0147	0.0022	0.0004
Q_e, calculated (mg/g)	5.57	9.42	19.65	20.12
Q_e, experimental (mg/g) at 60 min	4.55	8.37	14.32	8.46
R^2	0.9884	0.9998	0.9991	0.9278

4. Conclusion

In this study, magnetic adsorbent (M-A-C-BP) was successfully synthesized by combining Fe_3O_4 nanoparticles with the activated banana peel waste surface (A-C-BP). The adsorption isotherms of IC on the M-A-C-BP fitted the monolayer adsorption behavior of the Langmuir equation with the Q_m value of 8.72 mg/g obtained at 300.15 K. The M-A-C-BP showed effective IC adsorption with only 18% decrease in adsorption efficiency after 5 times of reusing. Kinetic experiments indicated that the adsorption system followed the pseudo-second-order kinetic model through chemisorption during the adsorption process. This study not only reports the method for the removal of the toxic pollutant from water, but it also brings an additional value to the banana peel waste.

Acknowledgments

This work was financially supported by the Thailand Research Fund (TRF) and Office of the Higher Education Commission (CHE) under grant number MRG6280017. This research work was partially supported by Chiang Mai University.

References

[1] H.R. Rashidi, N.M. Nik Sulaiman, N.A. Hashim, Batik industry synthetic wastewater treatment using nanofiltration membrane, Procedia Eng., 44 (2012) 2010–2012.
[2] M. Marcucci, G. Ciardelli, A. Matteucci, L. Ranieri, M. Russo, Experimental campaigns on textile wastewater for reuse by means of different membrane processes, Desalination, 149 (2002) 137–143.
[3] X. Chen, Z. Shen, X. Zhu, Y. Fan, W. Wang, Advanced treatment of textile wastewater for reuse using electrochemical oxidation and membrane filtration, Water SA, 31 (2005) 127–132.
[4] C. Suksaroj, M. Héran, C. Allègre, F. Persin, Treatment of textile plant effluent by nanofiltration and/or reverse osmosis for water reuse, Desalination, 178 (2005) 333–341.
[5] M. Marcucci, I. Ciabatti, A. Matteucci, G. Vernaglione, Membrane technologies applied to textile wastewater treatment, Ann. N. Y. Acad. Sci., 984 (2003) 53–64.
[6] S.H. Lin, W.Y. Liu, Continuous treatment of textile water by ozonation and coagulation, J. Environ. Chem. Eng., 120 (1994) 437–446.
[7] D.M. Reynolds, S.R. Ahmad, Rapid and direct determination of wastewater BOD values using a fluorescence technique, Water Res., 31(1997) 2012–2018.
[8] J. Bell, J.J. Plumb, C.A. Buckley, D.V. Stuckey, Treatment and decolorization of dyes in an anaerobic baffled reactor, J. Environ. Chem. Eng., 126 (2000) 1026–1032.
[9] T. Viraragahan, K.R. Ramakrishna, Fly ash for colour removal from synthetic dye solutions, Water Qual. Res. J. Can., 34 (1999) 505–517.
[10] V.K. Gupta, P.J.M. Carrott, M.M.L. Ribeiro Carrott, Suhas, Low-cost adsorbents: growing approach to wastewater treatment—a review, Crit. Rev. Env. Sci. Technol., 39 (2009) 783–842.
[11] B. Hu, Y. Ai, J. Jin, T. Hayat, A. Alsaedi, L. Zhuang, X. Wang, Efficient elimination of organic and inorganic pollutants by biochar and biochar-based materials, Biochar, 2 (2020) 47–64.
[12] N.S. Alharbi, B. Hu, T. Hayat, S.O. Rabah, A. Alsaedi, L. Zhuang, X. Wang, Efficient elimination of environmental pollutants through sorption-reduction and photocatalytic degradation using nanomaterials, Front. Chem. Sci. Eng., 14 (2020) 1124–1135.
[13] X. Liu, R. Ma, L. Zhuang, B. Hu, J. Chen, X. Liu, X. Wang, Recent developments of doped g-C_3N_4 photocatalysts for the degradation of organic pollutants, Crit. Rev. Env. Sci. Technol., (2020) (in Press), doi: 10.1080/10643389.2020.1734433.
[14] M. Hao, M. Qiu, H. Yang, B. Hu, X. Wang, Recent advances on preparation and environmental applications of MOF-derived carbons in catalysis, Sci. Total Environ., 760 (2021) 143333, doi: 10.1016/j.scitotenv.2020.143333.
[15] L. Yao, H. Yang, Z. Chen, M. Qiu, B. Hu, X. Wang, Bismuth oxychloride-based materials for the removal of organic pollutants in wastewater, Chemosphere, (2020) (in Press), doi: 10.1016/j.chemosphere.2020.128576.
[16] Y.-J. Zhang, Z.-J. Xing, Z.-K. Duan, M. Li, Y. Wang, Effects of steam activation on the pore structure and surface chemistry of activated carbon derived from bamboo waste, Appl. Surf. Sci., 315 (2014) 279–286.
[17] H.A. Le, L.T. Linh, S. Chin, J. Jurng, Photocatalytic degradation of methylene blue by a combination of TiO_2-anatase and coconut shell activated carbon, Powder Technol., 225 (2012) 167–175.
[18] A.K. Yadav, R. Abbassi, A. Gupta, M. Dadashzadeh, Removal of fluoride from aqueous solution and groundwater by wheat straw, sawdust and activated bagasse carbon of sugarcane, Ecol. Eng., 52 (2013) 211–218.
[19] Y.-D. Chen, M.-J. Huang, B. Huang, X.-R. Chen, Mesoporous activated carbon from inherently potassium-rich pokeweed by in situ self-activation and its use for phenol removal, J. Anal. Appl. Pyrolysis, 98 (2012) 159–165.
[20] M. Jain, V.K. Garg, K. Kadirvelu, Adsorption of hexavalent chromium from aqueous medium onto carbonaceous adsorbents prepared from waste biomass, J. Environ. Manage., 91 (2010) 949–957.
[21] B.H. Hameed, I.A.W. Tan, A.L. Admad, Adsorption isotherm, kinetic modeling and mechanism of 2,4,6-trichlorophenol on coconut husk-based activated carbon, Chem. Eng. J., 144 (2008) 235–244.
[22] I.O. Ali, A.M. Hassan, S.M. Shaaban, K.S. Soliman, Synthesis and characterization of ZSM-5 zeolite from rice husk ash and their adsorption of Pb^{2+} onto unmodified and surfactant-modified zeolite, Sep. Purif. Technol., 83 (2011) 38–44.
[23] A. Bhatnagar, W. Hogland, M. Marques, M. Sillanpää, An overview of the modification methods of activated carbon for its water treatment applications, Chem. Eng. J., 219 (2013) 499–511.
[24] S.M. Lamine, C. Ridha, H.-M. Mahfoud, C. Mouad, B. Lotfi, A.H. Al-Dujaili, Chemical activation of an activated carbon prepared from coffee residue, Energy Procedia, 50 (2014) 393–400.
[25] A.A. Ahmad, B.H. Hameed, Effect of preparation conditions of activated carbon from bamboo waste for real textile wastewater, J. Hazard. Mater., 173 (2010) 487–493.
[26] A.M. Aljeboree, A.N. Alshirifi, A.F. Alkaim, Kinetics and equilibrium study for the adsorption of textile dyes on coconut shell activated carbon, Arabian J. Chem., 10 (2017) S3381–S3393.
[27] I. Langmuir, The adsorption of gases on plane surfaces of glass mica and platinum, J. Am. Chem. Soc., 40 (1918) 1361–1403.
[28] P. Senthil Kumar, S. Ramalingam, S.D. Kirupha, A. Murugesan, T. Vidhyadevi, S. Sivanesan, Adsorption behavior of nickel(II) onto cashew nut shell: equilibrium, thermodynamics, kinetics, mechanism and process design, Chem. Eng. J., 167 (2011) 122–131.
[29] F.M. Pelissari, M.M. Andrade-Mahecha, P.J. do Amaral Sobral, F.C. Menegalli, Nanocomposites based on banana starch reinforced with cellulose nanofibers isolated from banana peels, J. Colloid Interface Sci., 505 (2017) 154–167.
[30] J. Dhumal, S. Bandgar, K. Zipare, G. Shahane, Fe_3O_4 ferrofluid nanoparticles: synthesis and rheological behavior, Int. J. Mater. Chem. Phys., 1 (2015) 141–145.
[31] A. Jafari, K. Boustani, S. Farjami Shayesteh, Effect of carbon shell on the structural and magnetic properties of Fe_3O_4 superparamagnetic nanoparticles, J. Supercond. Novel Magn., 27 (2014) 187–194.
[32] V. López-Ramón, C. Moreno-Castilla, J. Rivera-Utrilla, L.R. Radovic, Ionic strength effects in aqueous phase adsorption of metal ions on activated carbons, Carbon, 41 (2003) 2020–2022.

[33] F. Kremer, Fundamentals of interface & colloid science, Zeitschrift Für Physikalische Chemie, 199 (1997) 127–127.
[34] M.A.C. Stuart, G.J. Fleer, J. Lyklema, W. Norde, J.M.H.M. Scheutjens, Adsorption of ions, polyelectrolytes and proteins, Adv. Colloid Interface Sci., 34 (1991) 477–535.
[35] Z.H. Dastgerdi, S.S. Meshkat, M.D. Esrafili, Enhanced adsorptive removal of indigo carmine dye performance by functionalized carbon nanotubes based adsorbents from aqueous solution: equilibrium, kinetic, and DFT study, J. Nanostruct. Chem., 9 (2019) 323–334.
[36] S. Banerjee, M.C. Chattopadhyaya, Adsorption characteristics for the removal of a toxic dye, tartrazine from aqueous solutions by a low cost agricultural by-product, Arabian J. Chem., 10 (2017) S1629–S1638.
[37] H. Freundlich, W. Heller, The adsorption of *cis*- and *trans*-azobenzene, J. Am. Chem. Soc., 61 (1939) 2228–2230.
[38] T. Ngulube, J.R. Gumbo, V. Masindi, A. Maity, An update on synthetic dyes adsorption onto clay based minerals: a state-of-art review, J. Environ. Manage., 191 (2017) 35–57.